# Broadband Plasmonic Enhancement of High-Efficiency Dye-Sensitized Solar Cells by Incorporating Au@Ag@$SiO_2$ Core-Shell Nanocuboids

*Zhiyong Bao[†,1], Nianqing Fu[‡,*,1], Yongqiang Qin[†], Jun Lv[†], Yan Wang[†], Jijun He[§], Yidong Hou[‖], Chenyi Jiao[†], Yucheng Wu[†,*] and Jiyan Dai [§*]*

[†] School of Materials Science and Engineering, Hefei University of Technology, Hefei, 230009, P.R. China.

E-mail: wyc@tyut.edu.cn

[‡] School of Materials Science and Engineering, South China University of Technology, Guangzhou 510640, P.R. China.

E-mail: msnqfu@scut.edu.cn

[§] Department of Applied Physics, The Hong Kong Polytechnic University, Hung Hom, Kowloon, Hong Kong

E-mail: jiyan.dai@polyu.edu.hk

[‖]School of Physical Science and Technology, Sichuan University, Chengdu, 610064, P.R. China.

[1]These two authors (Zhiyong Bao and Nianqing Fu) contributed equally.



Bao, Z., Fu, N., Qin, Y., Lv, J., Wang, Y., He, J., ... & Dai, J. (2019). Broadband plasmonic enhancement of high-efficiency dye-sensitized solar cells by incorporating Au@ Ag@ SiO2 core–shell nanocuboids. ACS applied materials & interfaces, 12(1), 538-545.

**Abstract**

The introduction of plasmonic additives is an effective approach to improve the efficiency of dye-sensitized solar cells (DSSCs) since it may enhance the light absorption of solar devices. Herein, we designed broadband plasmonic absorption Au@Ag@$SiO_2$ nanocuboides (GSS NCs) as nanophotonic inclusions to achieve plasmon-enhanced DSSCs for the first time. These GSS NCs exhibit multiple broader and stronger plasmon resonances that can be tuned by adjusting structural morphologies to spectrally match the absorption band of the DSSC, particularly in weak absorption region of the dyes. By carefully tailoring the position of nanophotonic inclusions in the electrodes, both plasmonic near-field enhancement and far-field scattering effects can be fully exploited to boost up the light-harvesting and thus the performance of DSSCs. This leads to an average power conversion efficiency (PCE) of 10.34% for the optimized GSS NC incorporated cells, with a champion PCE of 10.58% recorded for one of the best plasmonic DSSC, corresponding to a PCE enhancement of 23.9% in comparison with control devices. The electromagnetic simulations are consistent with the experimental observations, further corroborating the synergistic effect of plasmonic enhancement in these DSSCs.

**Keywords:** dye-sensitized solar cells, plasmonic enhancement, core-shell nanostructure, broadband light-harvesting, light mangement

## 1. Introduction

As a powerful clean energy conversion technology, dye-sensitized solar cell (DSSC) has attracted much attention due to its high conversion efficiency, low manufacturing costs and environmentally friendly features.[1-12] Extending the response of photoactive layer to a broader range of solar spectrum is one of the most critical issues to achieve a highly efficient panchromatic solar cells. It is estimated that to obtain a device with PCE over 15%, an $I^-/I_3^-$ redox couple-based DSSC should harvest 80% of the input sunlight from 350 nm to 900 nm.[2] However, the most developed dyes, such as N3 and N719, demonstrate high light-extinction located at a wavelength range around 400-600 nm ($\lambda_{Hi}$), while the light absorbing capacity decreases drastically at the long wavelength over 600 nm. This makes the utilization of sunlight with low energy a significant challenge. Plasmonic effects have been broadly investigated as a means to address the limited light absorption of DSSC and other photovoltaic devices.[1-7] By altering the geometry, dimension, and composition of metal nanostructures, their optical characteristics can be tuned to either overlap with the sensitizer absorption and enhance light harvesting, or absorb light at a wavelength complementary to the sensitizer enabling broadband solar light capture in plasmonic solar cells. It was reported the development of plasmonic photovoltaics were based on diverse enhancement mechanisms. To date, the widely known localized surface plasmon resonance (LSPR) of noble metal nanoparticles (MNPs) has been employed to improve solar cell efficiency, by taking advantages of the LSPR-induced synergistic effect of plasmonic enhancement in light absorption,[2,10-14] increased far-field scattering,[15-16] and plasmon-induced hot carriers directly involved in photocurrent generation.[17-18] These plasmonic contributions played crucial roles in diverse photovoltaic systems, particularly DSSCs, in which the number of photons absorbed by sensitized dye molecules can notably increase through the incorporation of plasmonic MNPs. [19-24]

In a pioneering work of the applicability of plasmonic effects in DSSCs, Ag NPs deposited on $TiO_2$ films lead to improvement of the optical absorption of the dye molecules.[25] In 2016, Elbohy reported that incorporation of plasmonic Au nanostars into photoanodes for high efficiency DSSCs and the power conversion efficiency (PCE) of DSSCs was increased by 20% from 7.1% to 8.4% for N719.[26] Jang et al. incorporated Au@GO core-shell NPs into photoanodes to reduce charge recombination on the MNP surface and facilitate improved charge transport in DSSCs.[27] Recently, several studies have investigated the shape-dependent plasmonic effects of diverse Ag NPs embedded in the counter electrode on the enhanced performance of DSSCs.[28,29] However, the mostly used sphere Au or Ag NP only have a narrow-band absorbance (with a half-peak width commonly less than 100 nm) at ~530 nm and ~410 nm, respectively. Moreover, this LSPR response zone shows overlap with the strong absorption spectrum of N719 (Figure 1j), which makes the further plasmonic enhancement limited. Therefore, developing novel plasmonic nanostructures that sustain broadband LSPR excitations to enable panchromatic light absorption is desirable for high-efficiency solar cells.[2,10,30-33] Hammond and Belcher demonstrated wide-spectrum DSSCs using multiple core-shell plasmonic structures and achieved a PCE over 9.0%.[10,31] These studies revealed that increasing the utilization of the low energy solar spectrum, through employing noble MNPs with broad-band LSPR response, is more effective to improvement DSSCs efficiency, when compared with the spherical Au and Ag NPs. However, there are still limited reports on the incorporation of broadband absorption MNPs with tunable plasmon resonances in DSSC devices,[10,31-33] especially for the bimetal based MNPs with core-shell structures.[31-33]

The PCE enhancement is highly dependent on the geometric position of MNPs in plasmonic solar cells.[3,6,23] Therefore, by designing appropriate configuration, these MNPs can couple and scatter light very effectively, which is also highly desired. This may open up new horizons in the optimization strategy of photovoltaics. Another major concern associated with MNPs is that they can act as electron recombination centers in solar cells, when the MNPs

surface are exposed directly to the electrolyte. To avoid this issue, coating an insulating or semiconductor shell on core MNPs is usually necessary.[19,34,35] As it can (a) prevent the structural damage from the thermal treatment; (b) resist the noble metal being etched by the $I^-/I_3^-$ oxide couple layer, and (c) reduce charge recombination on the surface of metal NPs. Additionally, within nano-sized dielectric shell (~2 nm) the incident light is squeezed and hence the electromagnetic field could also be greatly enhanced.[35]

Taking note of the above observations, to improve the performance of solar cells the following issues should be emphasized: 1) By incorporating broadband plasmonic NPs in solar devices and extending the absorption edge of photoactive materials, this is a viable strategy to improve the light harvesting and maximizing the performance; 2) Optimizing the geometric configuration of plasmonic MNPs in solar cells could couple light from the far-field to the near-field at the absorbing dye molecules, thereby increasing the local electron-hole pair generation rate significantly; 3) Appropriate thickness of coating shell on MNPs could be a crucial factor in enhancing the performance of DSSCs by synergistically improving light absorption and facilitating charge separation. Therefore, in this work, we designed Au@Ag@$SiO_2$ nanocuboids (GSS NCs) with optimized geometric position in plasmonic cells to maximize the photocurrent and efficiency of the solar devices. GSS NCs showed remarkably enhanced absorption properties in the long-wavelength portion of the visible spectrum (600-750 nm) due to the coupling effect between Ag and Au, allowing broadband light harvesting. On the basis of comprehensive investigations, a high-efficiency DSSC was proposed based on a promising architecture. The plasmon-mediated DSSCs with 10.34% efficiency were achieved in our study. The protocol established here can be employed as a generalized strategy to develop other types of high-performance solar cells.

## 2. Results and Discussion

### 2.1. Structural and optical properties of synthesized GSS NCs

Au nanorods (GNRs) were synthesized employing the hexadecyltrimethylammonium bromide (CTAB) cationic surfactant as morphology controller and ascorbic acid as reductant. As shown in Figure 1, uniform GNRs with ~55 nm in length and 11 nm in width were obtained in the CTAB stabilized suspension. Then Ag shell was grown on the GNRs surface through reduction of $Ag^+$ by ascorbic acid. The thickness of the Ag shell can be readily controlled by adding various amount of $AgNO_3$ (*i.e.* 0.01 M, 0.02 M, 0.05 M and 0.1M), the corresponding samples are defined as Au@Ag-1, 2, 3 and 4. Figures 1 (a)-(d) show the transmission electron microscopy (TEM) images of typical Au@Ag with different Ag shell thickness. It reveals that the Ag thickness along the short axes increased remarkably from 7.5±0.8 nm to 23.7±2.4 nm, whereas a relative slow increase rate was observed along the long axes direction, from 3.0±0.5 nm to 10.2±2.2 nm, when the added $AgNO_3$ increases from 0.01 M to 0.1 M. As the asymmetric deposition of Ag shell, the length of the Au@Ag increases from ~61.5 to 75.1 nm, while the width increases dramatically from ~24.5 to 58.4 nm, leading to an aspect ratio decline from 2.5 to 1.3. Noted that a thin layer of $SiO_2$ (~5 nm) uniformly decorated on Au@Ag-1, 2, 3 and 4 samples by a typical Stöber method (Figure 1i), as defined by GSS NCs-1, 2, 3 and 4, respectively; their TEM images are shown in Figures 1(e)-(h). Figure 1j reveals the LSPR response and optical property of prepared GSS NC samples. There are four characteristic LSPR peaks exist in the 320-800 nm range. The peaks emerging in the 600-700 nm and 490-510 nm range correspond to the longitudinal and transverse LSPR excitations of GSS NCs, whereas the other two between around 320-430 nm represent the high-order LSPR modes. As shown in Figure 1k, the strongest longitudinal LSPR excitation GSS NCs can be effectively and continuously tuned from 705 nm to 621 nm (*i.e.* 705, 673, 644 and 621 nm, respectively) when the aspect ratio of GSS NC decreases. More importantly, the LSPR peaks

of GSS NCs, with an absorption band up to around 780 nm, are much broader than that of the plasmon Au and Ag spheres with absorption peak width around 100 nm.[28] Therefore, GSS NC nanostructures with tunable and broadband LSPR are achieved. As shown in Figure 1j the extinction spectra of the obtained GSS NCs are complementary to the weak absorption region (~400-500 nm and ＞600 nm) of N719 dyes, which is conducive to enhancing the utilization of light in the weak absorption region of DSSCs.

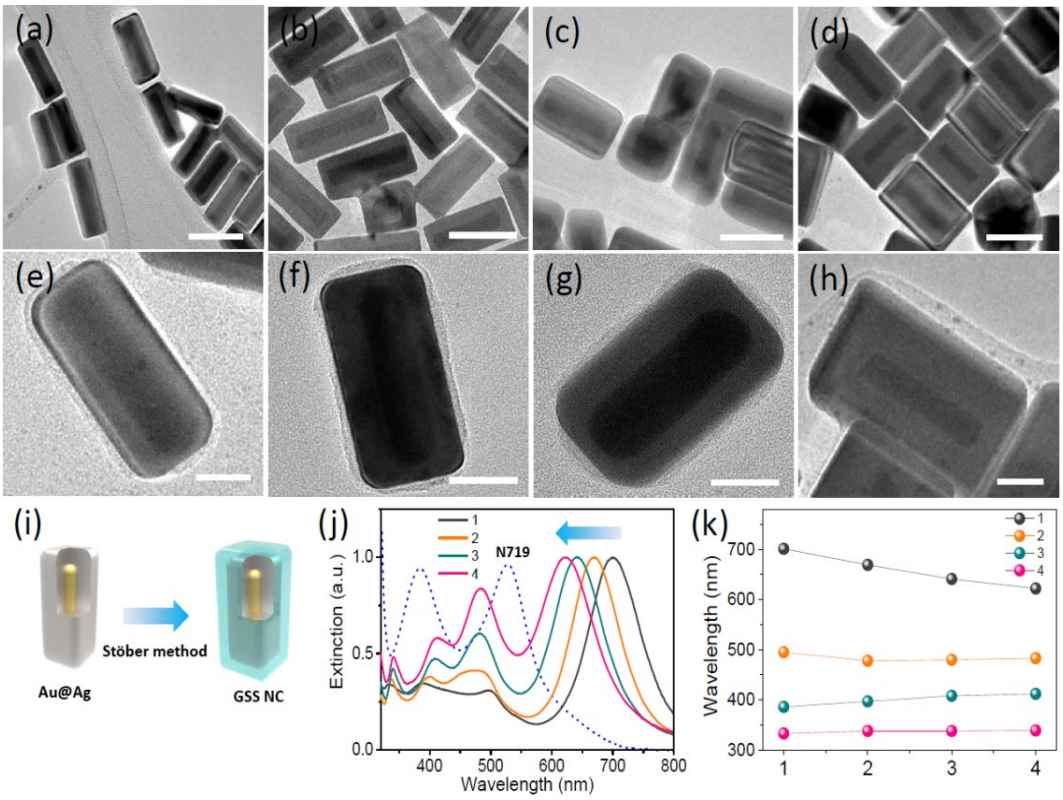


**Figure 1.** TEM images of prepared Au@Ag (a-d) and GSS NCs (e-h) with Ag shell increase. (i) The preparation process for GSS NCs. (j) The normalized extinction spectra and (k) statistical peak positions of four GSS NC samples. The blue dash line in (j) indicates the molecule's absorption light at a wavelength complementary to the GSS NCs in 350-800 nm range. The scale bars in (a)-(d) and (e)-(h) are 50 and 20 nm, respectively.

### 2.2. Broadband plasmonic absorption enhancements in GSS NC-incorporated DSSCs

The concentration of GSS NC incorporated in the photoactive layer of the prepared DSSCs was optimized individually to achieve maximized enhancement in device efficiency. The

optimized contents of GSS NC-1, 2, 3, and 4 in the photoactive layer are 0.87 wt%, 1.03 wt%, 1.25 wt% and 1.54 wt%, respectively (Figure S1). Figure 2a shows the *J-V* curves of the optimized devices and the corresponding photovoltaic parameters are tabulated in Table 1 for comparison. Control device was fabricated on the bare $TiO_2$ electrode without inclusion of any MNPs, which demonstrates a short-circuit current density ($J_{sc}$) of 15.57 mA/cm$^2$, an open-circuit photovoltage ($V_{oc}$) of 0.768 V and a fill factor (*FF*) of 0.714, leading to a PCE of 8.54%. Surprisingly, when the GSS NCs with intense and broad LSPR bands are incorporated into the devices, the $J_{sc}$ boosts significantly to 16.96-17.46 mA/cm$^2$, yielding PCE of 9.36%, 9.48%, 9.22%, and 9.03%, corresponding to efficiency enhancement of 9.6%, 11.0%, 8.0%, and 5.7%, respectively, for the GSS NC-1, 2, 3 and 4 based devices. On the other hand, the $V_{oc}$ of GSS NCs incorporated devices sufers a slight decrease. In fact, it is possible as the decreased *Voc* is resulted from the increased charge recombination in the photoande, which is similar to the previous cases of DSSC studies. [19,34] In our study, the incorporation of GSS NCs could result in the inhomogeneity of the $TiO_2$ film and thus lead to increased charge recombination (Figure S2), since the size of GSS NC is much larger than that for $TiO_2$ nanoparticles (~20 nm).

To reveal the factors governing the $J_{sc}$ and PCE enhancement, we measured the optical properties of various plasmonic NP incorporated $TiO_2$ films that sensitized by N719 dyes. As shown in Figure 2b, the absorption spectra of sensitized electrodes with different GSS NCs witness noticeable absorption improvement in the whole range of 400-750 nm for all cases, especially at the 400-500 nm and 600-750 nm representing the weak absorption ranges of N719. This remarkable enhanced light harvesting can eventually and effectively lead to the $J_{sc}$ increase and the improved efficiency of the solar cells.

As compared with UV-Vis light absorption, the incident photon-to-electron conversion efficiency (IPCE) is more pertinent to the photocurrent generation of DSSCs, since it takes the light harvest, electron injection, and charge collection into a comprehensive consideration.

The IPCE spectra and the relative IPCE enhancement (△IPCE/IPCE) as a function of wavelength are displayed in Figure 2c and d. It reveals that the devices without any plasmonic

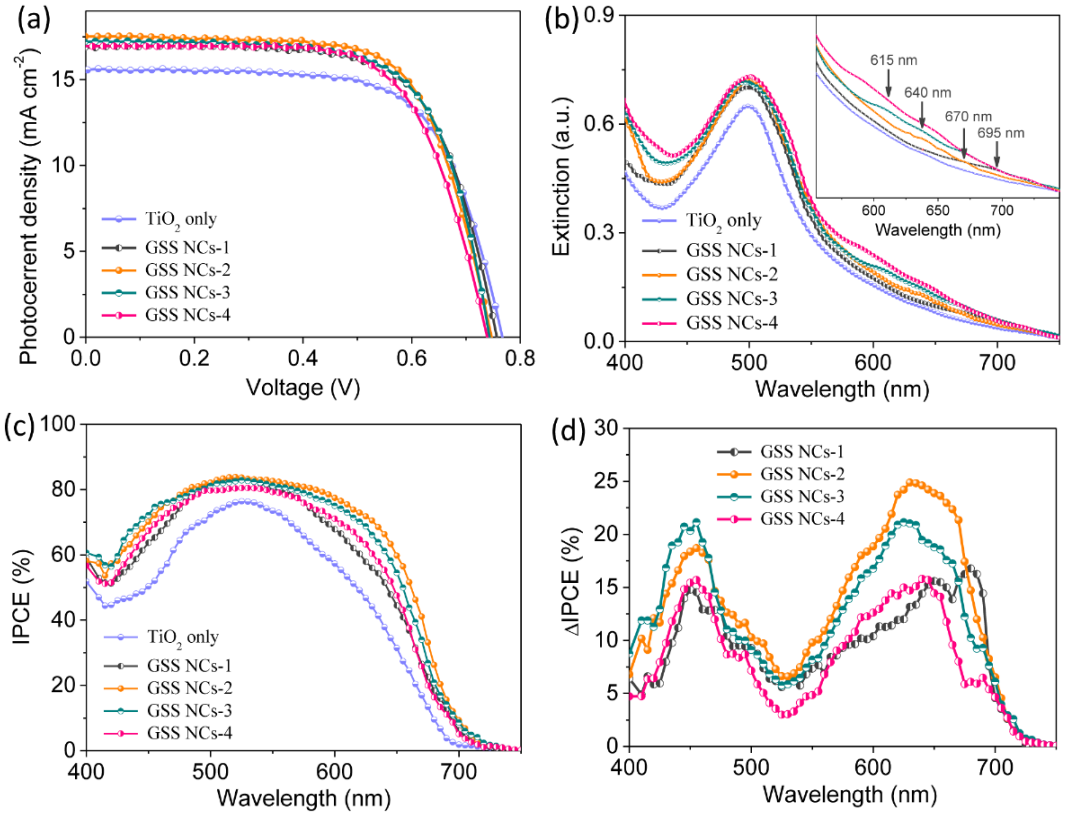


**Figure 2.** (a) The *J-V* curves of the optimized devices. (b) The extinction spectra of N719 sensitized electrodes with incorporation of different GSS NCs. (c) Measured IPCE spectra and (d) the relative IPCE enhancement (△IPCE/IPCE) as a function of wavelength of different devices.

**Table 1.** Photovoltaic parameters of GSS NC-incorporated DSSCs

| Devices | $J_{sc}$ [mA cm$^{-2}$] | $V_{oc}$ [V] | *FF* | PCE [%] | △PCE/PCE (%) | Dye-loading [$10^{-7}$×mol cm$^{-2}$] |
|---|---|---|---|---|---|---|
| $TiO_2$ only | 15.57 | 0.768 | 0.714 | 8.54 | / | 2.78 |
| GSS NCs-1 | 16.96 | 0.752 | 0.731 | 9.36 | 9.6 | 2.66 |
| GSS NCs-2 | 17.46 | 0.747 | 0.725 | 9.48 | 11.0 | 2.59 |
| GSS NCs-3 | 17.23 | 0.741 | 0.722 | 9.22 | 8.0 | 2.51 |
| GSS NCs-4 | 16.97 | 0.736 | 0.724 | 9.03 | 5.7 | 2.42 |
| Layer by layer | 18.81 | 0.748 | 0.735 | 10.34 | 21.0 | 2.35 |

MNP incorporation exhibit a relatively low IPCE and a remarkable IPCE decline at the wavelength ranges of 400-500 nm and 600-750 nm ($\lambda_{Lo}$); this is due to the relative low light extinction capacity at these zones. All devices incorporated with plasmonic MNPs demonstrate a considerable IPCE enhancement among 400-750 nm. Notably, a much remarkable increase in IPCE is observed in the $\lambda_{Lo}$ ranges for the GSS NCs incorporated cells, as compared with the enhancement at $\lambda_{Hi}$. For instance, the IPCE of the GSS NCs-2 cell is increased by ~22 and 27% at 450 nm and 650 nm, respectively, in contrast to only 8% at 530 nm. The ΔIPCE shown in Figure 2d illustrates a well wavelength-dependent IPCE increase. The ΔIPCE at the zones where the GSS NCs-X (X nm, X = 1, 2, 3 and 4) show the higher light extinction is obviously larger than that of its near-neighbor, indicating a real plasmonic effect based improvement. Therefore, it can be concluded that the remarkable enhancement of IPCE in the $\lambda_{Lo}$ ranges make the most significant contribution to the boosted $J_{sc}$ and PCE of the GSS NCs incorporated DSSCs.

**2.3. Plasmonic near-field enhancement in GSS NC-incorporated DSSCs**

Referring to the near-field nature of the plasmonic enhancement, a broader spatial distribution of the improved electromagnetic field will bring about more light-harvesting. The significant enhancement in the near field intensity is another key factor that enhances the light harvesting and IPCE of the GSS NC-incorporated DSSCs, apart from their stronger and tunable LSPR bands. As shown in Figure 3, the simulated extinction and scattering spectra of different GSS NCs demonstrate a continuous increase in extinction and scattering intensity (far-field effect) with Ag shell increase, consistent with the measured spectra of the GSS NCs in water (Figure 1j). To elaborate the LSPR effects of GSS NCs, we calculate the distributions of the electric field intensity for different plasmon modes. Typically, the electromagnetic field for longitudinal dipolar plasmon mode is much stronger than that for other plasmon modes

(Figure S3a-2d). Therefore, we chose the longitudinal plasmon mode for comparison and calculated electrical field enhancement of four GSS NCs samples under the excitation along the long axis of the Au core. The simulated field patterns shown in Figure S3a and S3e-g reveal that the plasmonic electric field can extend to tens of nanometers from the surface of the GSS NCs to the sensitizer.

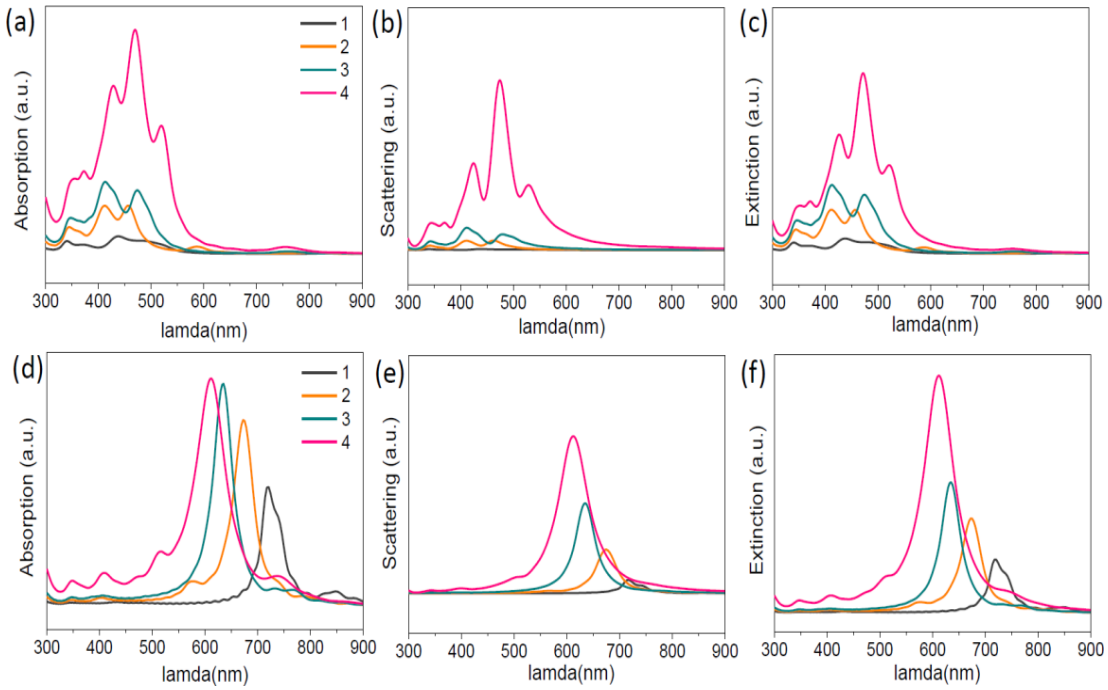


**Figure 3.** Simulated absorption, scattering and extinction spectra of GSS NCs along the x-direction polarization (a, b and c) and y-direction polarization (d, e and f) with varied Ag shell thickness (*i.e.* 3, 6, 9 and 16 nm).

For comparison, Figure 4 reveals the distributions of the electric field intensity on the transvers cross-sections of GSS NCs-2 and GSS NCs-4 at their longitudinal resonant wavelengths (more details are shown in Figure S4). We extract the scattering enhancement defined as the ratio $E/E_0$, where E ($E_0$) is the electric distribution with (without) MNP. It was shown both the near-field intensity and the field distribution size of longitudinal dipolar mode begin to decline significantly when the Ag shell thickness is larger than 9 nm. It's reasonable because not only the electric field is stronger when the radius of curvature of a nanoparticle is smaller, but also core-shell type bimetallic GSS NCs have more LSPR modes and larger

electric near-field due to the plasmon coupling from different metallic interfaces. As shown in Figure S4, the GSS NCs-1 exhibits the strongest near-field intensity and the largest field distribution size of longitudinal dipolar mode, while its near-field intensity and field distribution size of the dipolar mode is slightly larger than that of GSS NCs-2. On the contrary, the extinction of GSS NCs-2 is stronger than that for GSS NCs-1 (Figure 1j and Figure 3). Therefore, a higher efficiency is observed for the GSS NCs-2 incorporated device.

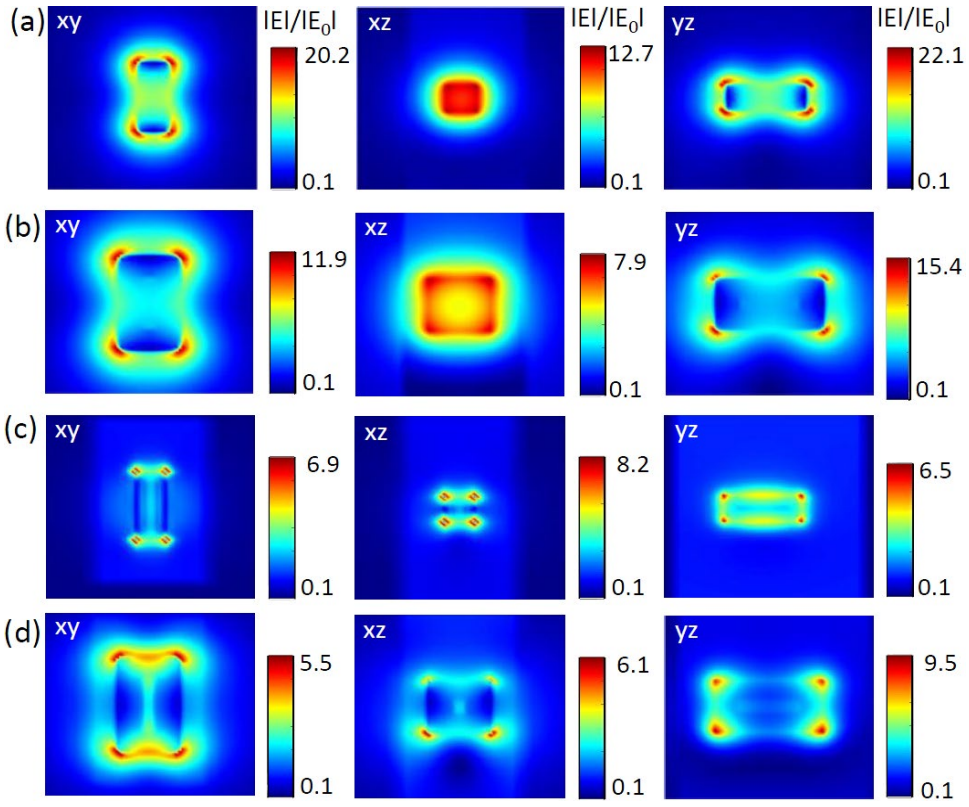


**Figure 4.** Calculated electric field intensity distributions and scattering enhancement ($E/E_0$) on the cross sections of GSS NC-2(a,c) and GSS NC-4(b,d) at the longitudinal (a,b) and transverse (c,d) resonant wavelengths, respectively.

### 2.4. Device optimization: effective light scattering management

To fully explore the efficient light management effect of GSS NCs in the solar devices and maximize the cell efficiency, we developed a layer-by-layer photoanode architecture shown in Figures 5a and 5c. The GSS NCs-1 (0.87 wt% incorporation) and GSS NCs-2 (1.04 wt% incorporation) were firstly chosen to be imbedded in the two lower layer since they give the

best plasmonic enhancement in photovoltaic performance as demonstrated above, while the GSS NCs-4 was chosen to be the scattering material since it possesses simultaneously large light scattering, high light extinction (Figure 1j and Figure 3). The inclusion of GSS NCs-4 in the plasmonic scattering layer was firstly optimized to be 4.2 wt.% (Figure S5). As schematically shown in Figure 5b, the light absorption of the photoanode was enhanced especially at the LSPR regions of MNPs, compared with that of the pristine $TiO_2$ case. This supports the enhancement in the light absorption by the plasmon resonance effect of MNPs in the nanocomposite photoanode. The strongly localized electromagnetic field and scattering intensity around the MNPs enhanced the optical path and absorption efficiency of the dye molecules,[36-38] resulting in the considerable increase in the photocurrent and PCE of the GSS NC-incorporated DSSCs. This light management strategy leads to an average PCE of 10.34% for the optimized GSS NC incorporated cells (Table 1). The champion device demonstrates a high PCE up to 10.58%, with $J_{sc}$, $V_{oc}$ and *FF* of 19.05 mA $cm^{-2}$, 0.753 V and 0.737, respectively (Figure 5d). In general, using the GSS NCs with broadened absorption band, stronger extinction capacity, significantly improved near-field effects and effective light scattering management one can obtain efficient plasmon-enhanced DSSCs with relatively high average PCE. Those results coherently demonstrate that the inclusion of the plasmonic GSS NCs with strong, broadband and tunable LSPR extinction into the active layer is a promising approach to increase the utilization of low-energy photons, leading to efficient panchromatic DSSCs with improved light harvesting efficiency. Meanwhile, exploiting the light scattering effect *via* a desirable structure can further enhance the photovoltaic performance, leading to a dual-enhancement effect of the plasmonic MNPs incorporated DSSCs.

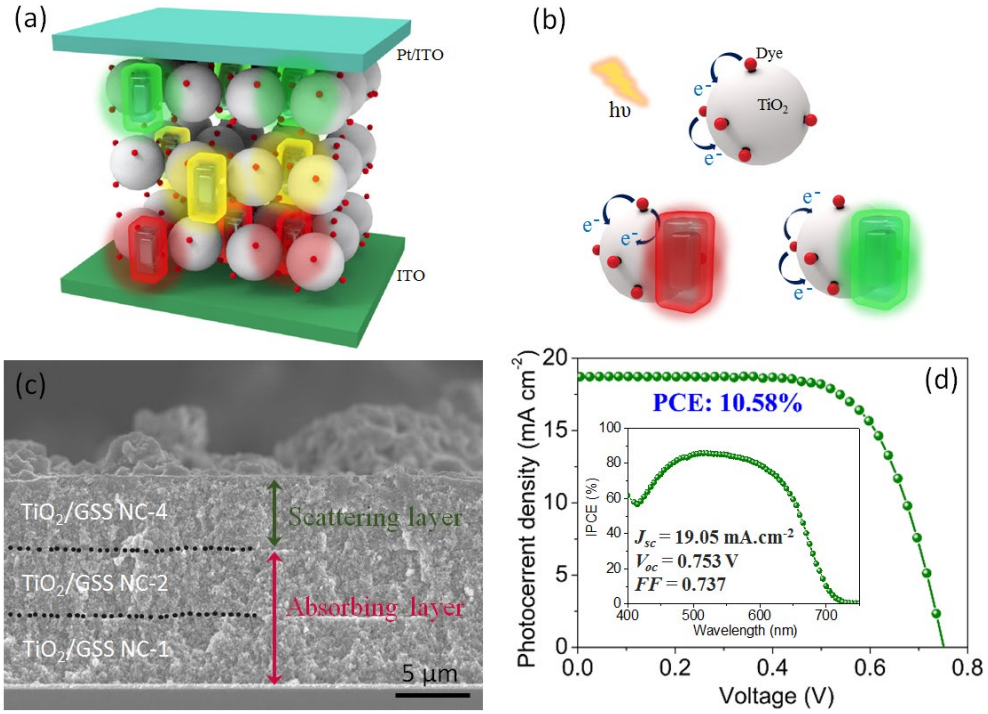


**Figure 5.** (a) The schematics of the GSS NC-incorporated DSSCs with the light management. (b) Schematic diagrams of the enhancement mechanisms of $TiO_2$ only and $TiO_2$-GSS NC composite. The MNPs with red and green rings represent the near- and far-field mechanism, respectively. (c) SEM of optimized layer-by-layer DSSC device structure and (d) The *J-V*, IPCE and other photovoltaic parameters of the champion devices.

## 2.5 Charge transport and transfer behaviors of GSS NC-incorporated DSSCs

The photoluminescence (PL) spectrum is performed to study the charge separation effect of Au@Ag@$SiO_2$-included DSSCs. Figure S6 shows the PL spectra for the N719 sensitized films with and without GSS NCs-2 incorporation, excited by the 585 nm wavelength radiation. The PL intensity for the Au@Ag@$SiO_2$ incorporated film shows a slight reduction compared to that of the pure $TiO_2$ one, which is similar to the previously reported work.[32] It is reasonable because the excitons excited from the dyes could be quenched by either energy transfer to MNPs through a radiative/nonradiative decay, or *via* induced charge separation.[39] In the Au@$TiO_2$ and Au@Ag@$TiO_2$ cases, the MNPs can act as electron acceptors to store electrons and thus accelerate the charge separation.[32,40] However, the PL dynamics in the Au@Ag@$SiO_2$-included DSSCs is quite different due to the insulating feature of the $SiO_2$

spacer. Moreover, in the surface energy transfer (SET) theory, when the transition energy of a dye matches that for a nearby MNP, the energy would release in the form of heat (nonradiative decay process).[19,41-43] However, in our case, judging by the remarkably improved $J_{sc}$ value in the Au@Ag@$SiO_2$ incorporated devices, charge transfer from the dyes to the MNPs is negligible. Hence, we assume that the ionization of the exciton (namely reduced exciton binding energy) would account for the improved charge separation in our case,[39] since the electromagnetic field nearby the GSS NCs is remarkably enhanced due to the LSPR effect.

To further study the charge transport and transfer behaviors of the Au@Ag@$SiO_2$ included DSSCs, the intensity modulated photocurrent spectroscopy (IMPS) and intensity modulated photovoltage spectroscopy (IMVS) measurements were conducted within the photoanodes. The electron transport time ($\tau_d$) and electron lifetime ($\tau_e$), which are associated with electron transport and charge recombination, respectively, can be estimated from $\tau = 1/2\pi f_{min}$. In the equation, $f_{min}$ is the frequency of the bottom of the semicircle at the IMPS or IMVS plots. As shown in Figure 6, the corresponding DSSCs based on pure $TiO_2$, GSS NCs-2 and layered GSS NCs (structure shown in Figure 5c) photoanodes demonstrate similar electron transport behaviors, with a $\tau_d$ of ~10 ms. The slight electron transport improvement of GSS NCs incorporated devices may result from the increased electron concentration in the $TiO_2$ film, due to the promoted light-harvesting efficiency. In contrast, the GSS NCs inclusion also lead to slightly decreased $\tau_d$ values, indicating the increased charge recombination in these solar cells. The IMVS results are in accordance with the decreased $V_{oc}$ values revealed by the *J-V* tests for the GSS NCs based devices. According the equation $\eta_{cc} = 1-\tau_d/\tau_d$, the electron collection efficiencies ($\eta_{cc}$) of pure $TiO_2$, GSS NCs-2 and GSS NCs included DSSCs are calculated to be 87.6%, 86.4% and 86.5%, respectively. The IMPS/IMVS results further indicate that the light-management induced by Au@Ag@$SiO_2$ will account for the improved device performance..

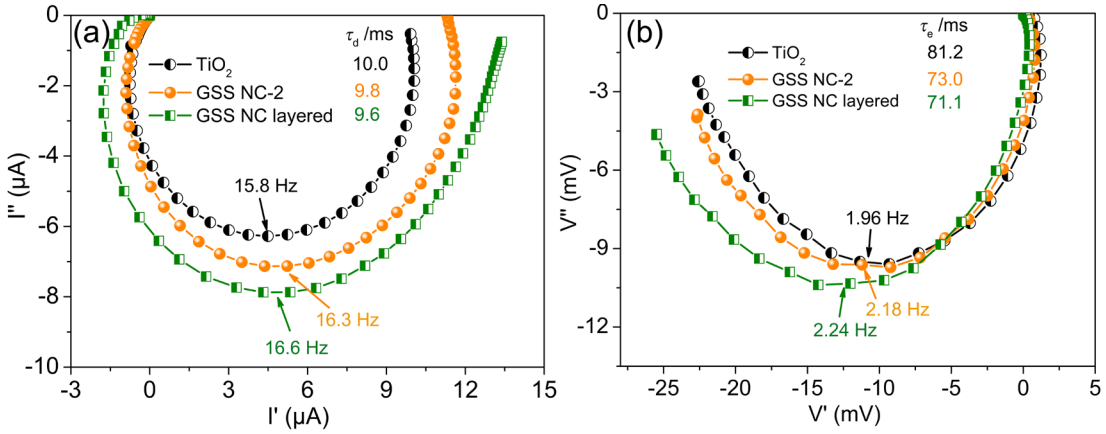


**Figure 6** The intensity modulated photocurrent spectroscopy (IMPS) (a) and intensity modulated photovoltage spectroscopy (IMVS) (b) of the DSSCs with pure $TiO_2$, GSS NCs-2 and layered GSS NCs (structure of Figure 5c) based photoanodes.

## 3. Conclusion

In summary, we propose an improved light harvesting and management strategy by using rationally-designed GSS NCs as plasmonic inclusions, aiming at achieving high-efficiency DSSCs. The GSS NCs exhibit multiple broader and stronger plasmon resonances that can be tuned by adjusting structural dimensions to spectrally match the absorption band of the dye molecules, particularly in its weak absorption region. Moreover, by designing an appropriate device structure, we can exploit the near field and light scattering effect in the DSSC devices simultaneously. In our wok, the plasmon-enhanced DSSCs with optimized location of nanophotonic inclusions in the electrodes result in an average PCE of 10.34% recorded for one of the best plasmonic DSSCs, corresponding to a PCE enhancement of 21% in comparison with control devices. This work paves a way for using broadband plasmonic absorption nanostructures with controllable optical properties in DSSCs as an alternative approach to effectively enhance device efficiencies.

## 4. Experimental Section

*Materials:* Titanium (IV) isopropoxide (97%, TTIP), acetic acid, methylamine (40% in methanol), hydroiodic acid (57 wt% in water), diethyl ether, hydrogen tetrachloroaurate (III)

hydrate ($HAuCl_4 \cdot 4H_2O$), sodium citrate ($C_6H_5Na_3O_7 \cdot 2H_2O$, 99%), *N, N* -Dimethylformamide (DMF, 99.9%) were obtained from Sigma-Aldrich. The Ru dye, cis-di(thiocyanato)-bis(2,2-bipyridyl-4,4-dicarboxylate) ruthenium(II) (N719), was purchased from Solaronix (Switzerland). All chemicals are used as received without further purification.

*Syntheses of Ag@Ag and Au@Ag@SiO₂ nanocuboids:* Au@Ag nanocuboid aqueous solutions ($2\times10^{-10}$ M) with four different Ag shell thicknesses (3, 6, 9 and 16 nm) were prepared by the method reported before.[44] The GSS NC nanostructures were synthesized *via* a modified Stöber method. A total of 10 ml of as-synthesized Au@Ag were centrifuged once at 6500 rpm. for 20 min to remove the excess CTAB. The precipitate was re-dispersed into 10 ml of deionized water, and 100 µl of 0.1 M NaOH aqueous solution was added to adjust the pH of the solution to 10-11. Then, 5, 7, 9, and 11 µL of 10 vol% TEOS methanol solution were added respectively under gentle stirring. The mixture solution was kept stirring for 12 h until the reactions were complete. The resultant nanostructures defined as GSS NCs-1, 2, 3 and 4 were washed twice at 5500 rpm. for 10 min to remove the CTAB and re-dispersed in water of the same volume. The sizes of the Au cores in the experiment were kept identical. Four types of newly synthesized GSS NC solutions were introduced into the devices.

*Electrodes and devices fabrication:* For $TiO_2$ paste preparation, organic-free anatase $TiO_2$ nanoparticles colloid with solid content of 18 wt.% was synthesized according to our previous work[7,45]. GSS NCs with various Ag shell thickness were washed by DI water and collected by 7000 rpm centrifugation for three times to remove the CTAB before adding into the $TiO_2$ paste. Appropriate amount of GSS NCs were dispersed in the $TiO_2$ paste by magnetic stirring and ultrasonic.

$TiO_2$ electrodes for DSSCs were fabricated according to our previous work with modification[7,45]. Shortly, $TiO_2$ electrodes for DSSCs were deposited by spreading the 18 wt.% $TiO_2$ paste with/without GSS NCs on the compact $TiO_2$ layer coated ITO substrates using the

doctor-blade technique. The thicknesses of the films were controlled to be ~15 μm. The dried $TiO_2$ electrodes were subjected to a fast anneal with a process of: 250 °C for 10 min (with a temperature ramp of 5 °C/min), 300 °C for 5 min, 400 °C for 5 min, and then cool down (5 °C/min). The sintered electrodes were subjected to a 20 MPa mechanical compression. For the DSSCs assembly, the $TiO_2$ electrodes were soaked in the 0.5 mM N719 ethanol solution overnight for dye-loading. After that, the electrodes were taken out and rinsed with ethanol. The sensitized photoanode, a drop of liquid electrolyte and a sputtered Pt-mirror counter electrode were sandwiched into DSSCs employing a 25 μm Surlyn 1702 film as spacer between the two electrodes. The liquid electrolyte is a 3-methoxypropionitrile solution composing of 0.5 M LiI, 0.05 M $I_2$, 0.3 M 1-methyl-3-hexylimidazolium iodide (HMII), 0.3 M *N*-methylbenzimidazole (NMB), and 0.5 M 4-*tert*-butylpyridine. The active area of the DSSCs was 0.09 $cm^{-2}$.

*Measurements and Characterization:* The optical properties of the N719 sensitized electrodes, the absorbance of the GSS NCs were investigated by an UV-vis spectrophotometer (Hitachi U-3010, Japan) equipping with an integrating sphere. The structure details of the GSS NCs were studied by transmission electron microscope (TEM, JEOL JEM-2100F). *I-V* curves were recorded using a Keithley 2420 source meter. The 1 sun AM 1.5 G illumination (100 mW $cm^{-2}$) was supplied by a 300 W solar simulator (Model 69911, Newport-Oriel Instruments, USA) and calibrated by a silicon reference cell (NIST) equipped with a power meter. The IPCE measurements were conducted on a Newport 2931-C power meter, employing a light source provided by a Newport 66902 solar simulator equipment with a Newport 74125 monochromator. The intensity modulated photocurrent spectroscopy (IMPS) and intensity modulated photovoltage spectroscopy (IMVS) were recored employing a Solartron 1255B frequency-response analyzer, using a green light emitting diode (LED, peak wavelength 520 nm).

*Electromagnetic simulations:* The full-wave simulations were conducted with a commercial finite-element solver (Comsol Multiphysics 4.3a with RF module), which is commonly used to simulate the LSPR properties of plasmonic MNPs. When performing the numerical simulations, the total-field scattering-field source was used to get the extinction cross sections as well as the electric field distributions at the longitudinal and transverse resonant wavelengths. In all calculations, the frequency dependent permittivity of Au and Ag were modeled using the experimental data of Johnson and Christy with linear interpolation. The simulation domain was finely meshed with the smallest size of 1.5 nm in the metal region to ensure the accuracy of the calculated results.

**Associated Content**

*Supporting Information

The Supporting Information of additional *J-V* photovoltaic parameters, SEM images, additional electric field simulation results, and PLspectra are available free of charge on the ACS Publications website at DOI:

**Author Information**

Corresponding Author

*E-mail: msnqfu@scut.edu.

*E-mail: wyc@tyut.edu.cn.

*E-mail: jiyan.dai@polyu.edu.hk

Zhiyong Bao and Nianqing Fu contributed equally to this work

**Notes**

The authors declare no competing financial interest.

**Acknowledgements**

This work was financially supported by National Natural Science Foundation of China (Grants Nos. 61604058, 51802066 and 51772072), Science and Technology Program of Guangzhou (201904010212) and the Fundamental Research Funds for the Central Universities of China (Grant No. JZ2019YYPY0023). Prof. Y. Wu thanks the financial support from the 111 Project "New Materials and Technology for Clean Energy" (B18018). Prof. J. Lv acknowledge the Opening Foundation of Guangxi Key Laboratory of Electrochemical Energy Materials (2018).

**References**

[1] Lu, M. Y.; Tsai, C. Y.; Chen, H. A.; Liang, Y. T.; Chen, K. P.; Gradečak, S.; Gwo, S.; Chen, L. J. Plasmonic Enhancement of Au Nanoparticle-Embedded Single-Crystalline ZnO Nanowire Dye-Sensitized Solar Cells. *Nano Energy* **2016**, *20*, 264-271.

[2] Chang, S.; Li, Q.; Xiao, X. D.; Wong, K. Y.; Chen, T. Enhancement of Low Energy Sunlight Harvesting in Dye-Sensitized Solar Cells Using Plasmonic Gold Nanorods. *Energy Environ. Sci*. **2012**, *5*, 9444-9448.

[3] Erwin, W. R.; Zarick, H. F.; Talbert, E. M.; Bardhan, R. Light Trapping in Mesoporous Solar Cells with Plasmonic Nanostructures. *Energy Environ. Sci*. **2016**, *9*, 1577-1601.

[4] Kawawaki, T.; Wang, H.; Kubo, T.; Saito, K.; Nakazaki, J.; Segawa, H.; Tatsuma, T. Efficiency Enhancement of PbS Quantum Dot/ZnO Nanowire Bulk-Heterojunction Solar Cells by Plasmonic Silver Nanocubes. *ACS Nano* **2015**, *4*, 4165-4172.

[5] Kochuveedu, S. T.; Jang, Y. H.; Kim, D. H.; A Study on the Mechanism for the Interaction of Light with Noble Metal-Metal Oxide Semiconductor Nanostructures for Various Photophysical Applications. *Chem. Soc. Rev*. **2013**, *42*, 8467-8493.

[6] Wang, Q.; Butburee, T.; Wu, X.; Chen, H.; Liu, G.; Wang, L. Enhanced Performance of Dye-Sensitized Solar Cells by Doping Au Nanoparticles into Photoanodes: a Size Effect Study. *J. Mater. Chem. A* **2013**, *1*, 13524-13531.

[7] Fu, N.; Bao, Z. Y.; Zhang, Y. L.; Zhang, G.; Ke, S.; Lin, P.; Dai, J.; Huang, H.; Lei, D. Y. Panchromatic Thin Perovskite Colar Cells with Broadband Plasmonic Absorption Enhancement and Efficient Light Scattering Management by Au@ Ag Core-Shell Nanocuboids. *Nano Energy* **2017**, *41*, 654-664.

[8] Li, W.; Ma, P.; Chen, F.; Xu, R.; Cheng, Z.; Yin, X.; Lin Y.; Wang, L. $CoSe_2$/Porous Carbon Shell Composites as High-Performance Catalysts toward Tri-iodide Reduction in Dye-Sensitized Solar Cells. *Inorg. Chem. Front.* **2019**, *6*, 2550-2557.

[9] Lu, W.; Jiang, R.; Yin, X.; Wang, L. Porous N-doped-Carbon Coated $CoSe_2$ Anchored on Carbon Cloth as 3D Photocathode for Dye-Sensitized Solar Cell with Efficiency and Stability Outperforming Pt. *Nano Research* **2019**, *12 ,* 159-163.

[10] Dang, X. N.; Qi, J. F.; Klug, M. T.; Chen, P. Y.; Hammond, P.T.; Belcher, A. M.; Yun, D. S.; Fang, N. X. Tunable Localized Surface Plasmon-Enabled Broadband Light-Harvesting Enhancement for High-Efficiency Panchromatic Dye-Sensitized Solar Cells. *Nano Lett*. **2013**, *13*, 637-642.

[11] Zhou, L.; Yu, X. Q.; Zhu, J. Metal-Core/Semiconductor-Shell Nanocones for Broadband Solar Absorption Enhancement. *Nano Lett*. **2014**, *14*, 1093-1098.

[12] Fu, N.; Liu, Y.; Liu, Y. C.; Lu, W.; Zhou, L. M.; Peng, F.; Huang, H. Facile Preparation of Hierarchical $TiO_2$ Nanowire-Nanoparticle/Nanotube Architecture for Highly Efficient Dye-Sensitized Solar Cells. *J. Mater. Chem. A* **2015**, *3*, 20366-20374.

[13] Zhou, L.; Tan, Y. L.; Ji, D. X.; Zhu, B.; Zhang, P.; Xu, J.; Gan, Q. Q.; Yu, Z. F.; Zhu, J. Self-Assembly of Highly Efficient, Broadband Plasmonic Absorbers for Solar Steam Generation. *Sci. Adv*. **2016**, *2*, e1501227.

[14] Tang, M. Y.; Zhou, L.; Gu, S.; Zhu, W. D.; Wang, Y.; Xu, J.; Deng, Z. T.; Yu, T.; Lu, Z. D.; Zhu, J. Fine-Tuning the Metallic Core-Shell Nanostructures for Plasmonic Perovskite Solar Cells. *Appl. Phys. Lett*. **2016**, *109*, 183901.

[15] Baek, S. W.; Park, G.; Noh, J.; Cho, C.; Lee, C. H.; Seo, K.; Song, H.; Lee, J. Y. Au@Ag Core-Shell Nanocubes for Efficient Plasmonic Light Scattering Effect in Low Bandgap Organic Solar Cells. *ACS Nano* **2014**, *8*, 3302-3312.

[16] Chou, C. H.; Chen, F. C. Plasmonic Nanostructures for Light Trapping in Organic Photovoltaic Devices. *Nanoscale* **2014**, *6*, 8444-8458.

[17] Arquer, F. P. G.; Mihi, A.; Kufer, D.; Konstantatos, G. Photoelectric Energy Conversion of Plasmon-Generated Hot Carriers in Metal-Insulator-Semiconductor Structures. *ACS Nano* **2013**, *7*, 3581-3588.

[18] Yuan, Z.; Wu, Z.; Bai, S.; Xia, Z.; Xu, W.; Song, T.; Wu, H.; Xu, L.; Si, J.; Jin, Y.; Sun, B. Hot-Electron Injection in a Sandwiched $TiO_x$-Au-$TiO_x$ Structure for High-Performance Planar Perovskite Solar Cells. *Adv. Energy Mater*. **2015**, *5*, 1500038.

[19] Yip, C.T.; Liu, X.; Hou, Y.; Xie, W.; He, J.; Schlücker, S.; Lei, D.Y.; Huang, H. Strong Competition Between Electromagnetic Enhancement and Surface-Energy-Transfer Induced Quenching in Plasmonic Dye-Sensitized Solar Cells: a Generic Yet Controllable Effect. *Nano Energy* **2016**, *26*, 297-304.

[20] Brown, M. D.; Suteewong, T.; Kumar, R. S. S.; D'Innocenzo, V.; Petrozza, A.; Lee, M. M.; Wiesner, U.; Snaith, H. J. Plasmonic Dye-Sensitized Solar Cells Using Core-Shell Metal-Insulator Nanoparticles. *Nano Lett*. **2011**, *11*, 438-445.

[21] Bai, L.; Liu, X.; Li, M.; Guo, K.; Luoshan, M.; Zhu, Y.; Jiang, R.; Liao, L.; Zhao, X. Plasmonic Enhancement of the Performance of Dye-Sensitized Solar Cells by Incorporating Hierarchical $TiO_2$ Spheres Decorated with Au Nanoparticles. *Electrochim. Acta* **2016**, *190,* 605-611.

[22] Fu, N.; Jiang, X.; Chen, D.; Duan, Y.; Zhang, G.; Chang, M.; Fang, Y.; Lin, Y. Au/$TiO_2$ Nanotube Array Based Multi-hierarchical Architecture for Highly Efficient Dye-Sensitized Solar Cells. *Journal of Power Sources* **2019**, *439*, 227076.

[23] Hou, W.; Pavaskar, P.; Liu, Z.; Theiss, J.; Aykol, M.; Cronin, S. B. Plasmon Resonant Enhancement of Dye Sensitized Solar Cells. *Energy Environ. Sci*. **2011**, *4*, 4650-4655.

[24] Naphade, R. A.; Tathavadekar, M.; Jog, J. P.; Agarkar, S.; Ogale, S. Plasmonic Light Harvesting of Dye-Sensitized Solar Cells by Au-Aanoparticle Loaded $TiO_2$ Nanofibers. *J. Mater. Chem. A* **2014**, *2*, 975-984.

[25] Wen, C.; Ishikawa, K.; Kishima, M.; Yamada, K. Effects of Silver Particles on the Photovoltaic Properties of Dye-Sensitized $TiO_2$ Thin Films. *Sol. Energy Mater. Sol. Cells* **2000**, *61*, 339-351.

[26] Elbohy, H.; Kim, M. R.; Dubey, A.; Reza, K. M.; Ma, D.; Zai, J.; Qian, X.; Qiao, Q. Incorporation of Plasmonic Au Nanostars into Photoanodes for High Efficiency Dye-Sensitized Solar Cells. *J. Mater. Chem. A* **2016**, *4*, 545-551.

[27] Jang, Y. H.; Rani, A.; Quan, L. N.; Adinolfi, V.; Kanjanaboos, P.; Ouellette, O.; Son, T.; Jang, Y. J.; Chung, K.; Kwon, H.; Kim, D.; Kim, D. H.; Sargent, E. H. Graphene Oxide Shells on Plasmonic Nanostructures Lead to High-Performance Photovoltaics: A Model Study Based on Dye-Sensitized Solar Cells. *ACS Energy Lett*. **2017**, *2,* 117-123.

[28] Hwang, H. J.; Joo, S. J.; Patil, S. A.; Kim, H. S. Efficiency Enhancement in Dye-Sensitized Solar Cells Using the Shape/Size-Dependent Plasmonic Nanocomposite Photoanodes Incorporating Silver Nanoplates. *Nanoscale* **2017**, *9*, 7960-7969.

[29] Ganeshan, D.; Xie, F.; Sun, Q.; Li, Y.; Wei, M. Plasmonic Effects of Silver Nanoparticles Embedded in the Counter Electrode on the Enhanced Performance of Dye-Sensitized Solar Cells. *Langmuir* **2018**, *34*, 5367-5373.

[30] Xu, Q.; Liu, F.; Liu, Y.; Cui, K.; Feng, X.; Zhang, W.; Huang, Y. Broadband Light Absorption Enhancement in Dye-Sensitized Solar Cells with Au-Ag Alloy Popcorn Nanoparticles. *Sci. Rep*. **2013**, *3*, 2112.

[31] Qi, J.; Dang, X.; Hammond, P. T.; Belcher, A. M. Highly Efficient Plasmon-Enhanced Dye-Sensitized Solar Cells Through Metal@ Oxide Core-Shell Nanostructure. *ACS Nano* **2011**, *5*, 7108-7116.

[32] Dong, H.; Wu, Z.; El-Shafei, A.; Xia, B.; Xi, J.; Ning, S.; Jiao, B.; Hou, X. Ag-Encapsulated Au Plasmonic Nanorods for Enhanced Dye-Sensitized Solar Cell Performance. *J. Mater. Chem. A* **2015**, *3*, 4659-4668.

[33] Liu, Q.; Sun, Y.; Yao, M.; Xu, B.; Liu, G.; Hussain, M. B.; Jiang, K.; Li, C. Au@Ag@$Ag_2S$ Heterogeneous Plasmonic Nanorods for Enhanced Dye Sensitized Solar Cell Performance. *Sol. Energy* **2019**, *185*, 290-297.

[34] Choi, H.; Chen, W. T.; Kamat, P. V. Know Thy Nano Neighbor. Plasmonic Versus Electron Charging Effects of Metal Nanoparticles in Dye-Sensitized Solar Cells. *ACS Nano* **2012**, 6, 4418-4427.

[35] Li, J. F.; Huang, Y. F.; Ding, Y.; Yang, Z. L.; Li, S. B.; Zhou, X. S.; Fan, F. R.; Zhang, W.; Zhou, Z. Y.; Wu, D. Y.; Ren, B.; Wang, Z. L.; Tian, Z. Q. Shell-Isolated Nanoparticle-Enhanced Raman Spectroscopy. *Nature* **2010**, *464*, 392-395.

[36] Li, X.; Choy, W. C. H.; Lu, H.; Sha, W. E.; Ho, A. H. P. Efficiency Enhancement of Organic Solar Cells by Using Shape-Dependent Broadband Plasmonic Sbsorption in Metallic Nanoparticles. *Adv. Funct. Mater*. **2013**, *23*, 2728-2735.

[37] Jeong, N. C.; Prasittichai, C.; Hupp, J. T. Photocurrent Enhancement by Surface Plasmon Resonance of Silver Nanoparticles in Highly Porous Dye-Sensitized Solar Cells. *Langmuir* **2011**, *27*, 14609-14614.

[38] Rand, B. P.; Peumans, P.; Forrest, S. R. Long-Range Absorption Enhancement in Organic Tandem Thin-Film Solar Cells Containing Silver Nanoclusters. *J. Appl. Phys*. **2004**, *96*, 7519-7526.

[39] Zhang, W.; Saliba, M.; Stranks, S. D.; Sun, Y.; Shi, X.; Wiesner, U.; Snaith, H. J. Enhancement of Perovskite-Based Solar Cells Employing Core-Shell Metal Nanoparticles. *Nano Lett.* **2013**, *13*, 4505-4510.

[40] Naphade, R. A.; Tathavadekar, M.; Jog, J. P.; Agarkar, S.; Ogale, S. Plasmonic Light Harvesting of Dye Sensitized Solar Cells by Au-Nanoparticle Loaded $TiO_2$ Nanofibers. *J. Mater. Chem. A* **2014**, *2*, 975-984.

[41] Dulkeith, E.; Morteani, A. C.; Niedereichholz, T.; Klar, T. A.; Feldmann, J. Fluorescence Quenching of Dye Molecules near Gold Nanoparticles: Radiative and Nonradiative Effects. *Phys. Rev. Lett.* **2002**, *89*, 203002.

[42] Ni, W. H.; An, J.; Lai, C. W.; Ong, H. C.; Xu, J. B. Emission Enhancement from Metallodielectric-Capped ZnO Films. *J. Appl. Phys.* **2006**, *100*, 026103.

[43] Jin, S.; DeMarco, E.; Pellin, M. J.; Farha, O. K.; Wiederrecht, G. P.; Hupp, J. T. Distance-Engineered Plasmon-Enhanced Light Harvesting in CdSe Quantum Dots. *J. Phys. Chem. Lett.* **2013**, *4*, 3527-3533.

[44] Bao, Z. Y.; Zhang, W.; Zhang, Y.; He, J.; Dai, J.; Yeung, C. T.; Law, G. L.; Lei, D. Y. Interband Absorption Enhanced Optical Activity in Discrete Au@ Ag Core-Shell Nanocuboids: Probing Extended Helical Conformation of Chemisorbed Cysteine Molecules. *Angew. Chem. Inter. Ed*. **2017**, *56*, 1283-1288.

[45] Fu, N.; Huang, C.; Liu, Y.; Li, X.; Lu, W.; Zhou, L.; Peng, F.; Liu, Y.; Huang, H. Organic-Free Anatase $TiO_2$ Paste for Efficient Plastic Dye-Sensitized Solar Cells and Low Temperature Processed Perovskite Solar Cells. *ACS Appl. Mater. & Interfaces* **2015**, *7*, 19431-19438.

## Table of Content